High Power Laser Science and Engineering, (2024), Vol. 12, e60, 10 pages.
doi:10.1017/hpl.2024.37

HIGH POWER LASER SCIENCE AND ENGINEERING

RESEARCH ARTICLE

Tunable X-ray frequency comb generation at the Shanghai soft X-ray Free-Electron Laser facility

Lanpeng Ni[1,3,4], Yaozong Xiao[1,3], Zheng Qi[2], Chao Feng[2,3], and Zhentang Zhao[2,3]

[1] *Shanghai Institute of Applied Physics, Chinese Academy of Sciences, Shanghai, China*

[2] *Shanghai Advanced Research Institute, Chinese Academy of Sciences, Shanghai, China*

[3] *University of Chinese Academy of Sciences, Beijing, China*

[4] *Zhangjiang Laboratory, Shanghai, China*

(Received 17 April 2024; revised 23 May 2024; accepted 3 June 2024)

Abstract

X-ray frequency combs (XFCs) are of great interest in many scientific research areas. In this study, we investigate the generation of high-power tunable XFCs at the Shanghai soft X-ray Free-Electron Laser facility (SXFEL). To achieve this, a chirped frequency-beating laser is employed as the seed laser for echo-enabled harmonic generation of free-electron lasers. This approach enables the formation of an initial bunching of combs and ultimately facilitates the generation of XFCs under optimized conditions. We provide an optical design for the chirped frequency-beating seed laser system and outline a method to optimize and set the key parameters that meets the critical requirements for generating continuously tunable XFCs. Three-dimensional simulations using realistic parameters of the SXFEL demonstrate that it is possible to produce XFCs with peak power reaching 1.5 GW, central photon energy at the carbon K edge (~284 eV) and tunable repetition frequencies ranging from 7 to 12 THz. Our proposal opens up new possibilities for resonant inelastic X-ray scattering experiments at X-ray free-electron laser facilities.

Keywords: chirped frequency beating; echo-enabled harmonic generation; free-electron laser; optical frequency combs

1. Introduction

An optical frequency comb (OFC) is a spectral structure composed of a series of equally spaced discrete spectral lines in the frequency domain[1], where the spectral lines are also called comb teeth. The interval between comb teeth corresponds to the repetition frequency of the pulses for conventional OFCs[2]. In practice, the conventional OFC is used as an accurate absolute optical frequency measuring ruler[1,3], which can establish a strong connection between microwave and optical frequencies[4,5] and provide a reliable and accurate research tool for many scientific research areas, such as light wave microwave frequency synthesis, precision ranging, precision spectroscopy, astronomy and communication[6–10]. High-power OFCs can also be used for resonant inelastic X-ray scattering (RIXS) and terabit-level coherent optical communication[11,12]. Generally, conventional OFCs are mainly generated by a femtosecond mode-locked laser, which can cover the infrared to ultraviolet regime[13,14]. In addition, the high-order harmonic generation (HHG) technique can produce OFCs in the extreme ultraviolet (EUV) regime[15–17]. However, due to the inherent nature of HHG, achieving OFCs at short wavelength is still a challenge[18], and the pulse energy of the OFCs from HHG is severely limited to a few nanojoules (~nJ).

As an internationally recognized advanced light source, free-electron lasers (FELs) with ultra-high brightness, ultrashort pulses, full spatial coherence and wide tunability have enabled research in many scientific frontiers in physics, chemistry, biology and material science[19–23]. FELs are driven by a high-quality relativistic electron beam passing through a field-periodically varying magnetic structure, termed an undulator. The most common mechanism of FELs is self-amplified spontaneous emission (SASE)[24,25], in which the initial spontaneous emission signal starts from the shot noise of the electron beam and becomes coherently amplified towards ultrabright X-ray radiation bursts. However, the longitudinal coherence of SASE pulses is constrained by the radiation slippage occurring within the FEL gain length. The concept of self-seeding schemes

Correspondence to: C. Feng and Z. Qi, Shanghai Advanced Research Institute, Chinese Academy of Sciences, Shanghai 201210, China. Emails: fengc@sari.ac.cn (C. Feng); qiz@sari.ac.cn (Z. Qi)

has been introduced to enhance the longitudinal coherence, albeit at the cost of shot-to-shot intensity variations[26,27]. There are also external seeded FEL mechanisms[28], which employ external seed lasers to modulate the electron beam and initiate the X-ray free-electron laser (XFEL) process. The seeded FELs can inherit the properties of the seed laser and deliver XFEL pulses with well-preserved longitudinal coherence and stability. Notable examples include high-gain harmonic generation (HGHG)[29,30] and echo-enabled harmonic generation (EEHG)[31–33]. Generally, EEHG employs two seed lasers to finely tune the phase space of the electron beam, through which very high harmonics of the seed laser can be generated with a relatively small energy modulation. This makes EEHG suitable for short wavelength and fully coherent FEL generation. The lasing of EEHG at short wavelength has been achieved at the Trieste FERMI[34] and Shanghai soft X-ray Free-Electron Laser facility (SXFEL)[35,36].

Seeded FELs also hold great promise for generating high-power X-ray frequency combs (XFCs). In recent years, several methods have been proposed to generate high-power XFCs based on either self-seeding[37] or external seeding[38,39]. In these methods, the repetition frequency of the pulse train depends on the wavelength of the seed laser, as they lack the ability to adjust the repetition frequency of the XFCs dynamically and continuously. In addition, relying on a chirped frequency-beating seed laser, the approach presented by Xu *et al.*[40] offers the advantages of a relatively simple setup and flexible control over the repetition frequencies of the XFCs. However, detailed analysis of the critical requirements on the generation of the XFCs regarding various parameters of the seed laser is missing.

SXFEL is the first X-ray FEL user facility in China[41]. Besides SASE, various seeding schemes, such as the EEHG and EEHG cascade, have also been adopted for the better performance of the facility. In this paper we focus on the study of generating high-power continuously tunable XFCs based on the SXFEL. We have designed an optical system for the generation of the chirped frequency-beating seed laser, which is used as the second seed laser in the EEHG scheme and helps to create the initial bunching combs. We explain the principles of generating XFCs using the seed laser in the EEHG-FEL and outline a method to optimize and set the key parameters that meets the critical requirements. Theoretical analysis and numerical simulations are given out to demonstrate the potential performance of our method. This paper is organized as follows: the method and principles are illustrated in Section 2, the simulation results are presented in Section 3 and the discussion and final conclusions are given in Section 4.

2. Method and principle

The schematic layout of our method is illustrated in Figure 1; it mainly consists of an EEHG-FEL setup in the SXFEL and a chirped frequency-beating seed laser system.

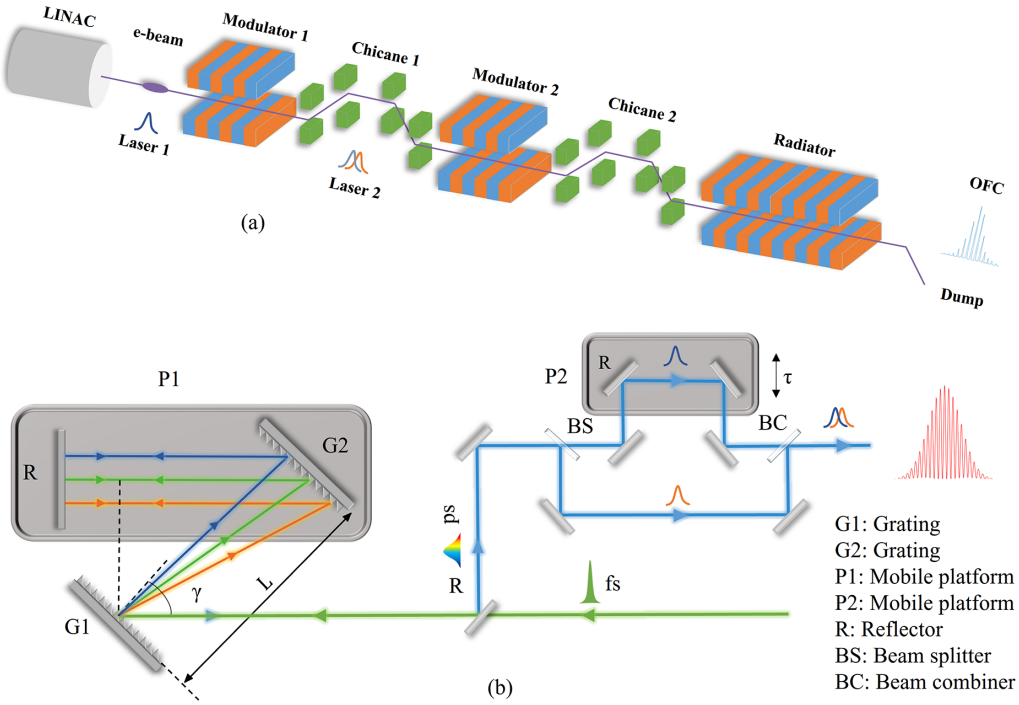

Figure 1. Schematic layout of the proposed method (a) and the design of the chirped frequency-beating seed laser system (b). The movement direction of the movable platform is indicated by black bidirectional arrows.

https://doi.org/10.1017/hpl.2024.37 Published online by Cambridge University Press

The EEHG-FEL setup consists of a two-stage modulation-dispersion section (modulator-chicane) and one radiation section (radiator), as shown in Figure 1(a). Through the EEHG-FEL setup, fully coherent XFEL radiation pulses can be generated at several tens of harmonics of the seed laser. Two external seed lasers (Laser 1, Laser 2) are needed in the configuration to interact with the electron beam and form the required finest bunching structure. Among them, Laser 2 is dedicated to being a chirped frequency-beating seed laser, and through this mode-locked bunching combs can be imprinted into the electron beam and can be further used to generate high-power XFC radiation bursts.

The chirped frequency-beating seed laser system mainly includes a pair of parallel gratings (G1, G2), a beam splitter (BS), an optical delay line, a beam combiner (BC) and so on, as shown in Figure 1(b). Firstly, the laser emitted from the laser source (~fs) propagates along the green line and undergoes dispersion through the parallel gratings, introducing linear chirping and temporal broadening. Subsequently, the chirped laser is altered at the optical path height by the leftmost reflectors and reflected so that it passes through the parallel gratings again. The chirped laser (~ps) is then introduced into the upper right-hand blue line by the reflector and split into two identical beams by the BS. Afterwards, an optical delay line introduces a time delay, causing these two beams to intersect at the BC and form a chirped frequency-beating seed laser (Laser 2).

2.1. Chirped frequency-beating laser

To clearly express the generation principle of Laser 2, we assume an initial Gaussian optical pulse with center frequency ω_0, root mean square (RMS) bandwidth σ_{in} and amplitude A. The electrical field of the initial laser can be expressed as follows:

$$E_{\text{in}} = Ae^{-\left(i\omega_0 t+\frac{t^2}{\sigma_{\text{in}}^2}\right)}. \tag{1}$$

Under the action of a parallel grating pair (a linear dispersive medium), the phase of the laser pulses is modulated, and the Taylor expansion of the modulated phase at the center frequency ω_0 can be written as follows:

$$\varphi(\omega) = \varphi(\omega_0) + \varphi_1(\omega-\omega_0) + \varphi_2\frac{(\omega-\omega_0)^2}{2!} + \varphi_3\frac{(\omega-\omega_0)^3}{3!} + \cdots, \tag{2}$$

where φ_1 (also known as τ_0) represents the group delay at ω_0, $1/\varphi_2$ (also written as μ) denotes the carrier frequency sweep rate and $\varphi_3/6$ (also referred to as β) signifies the cubic phase modulation. Higher order dispersion, which has minimal impact on femtosecond lasing, will be ignored in the following derivations[42]. After propagation through the parallel grating pair, the electrical field of the laser can be given by the following[42–44]:

$$E_{\text{out}} = A\sqrt{\frac{\sigma_{\text{in}}}{\sigma_{\text{out}}}}\exp\left(-\frac{t^2}{\sigma_{\text{out}}^2}\right)\exp\left(-i\left(\varphi_0'+\omega_0 t+\alpha t^2+\beta t^3\right)\right), \tag{3}$$

where σ_{out} is the length of the laser after broadening by the parallel grating pair; when $\sigma_{\text{out}} \gg \sigma_{\text{in}}$, then $\sigma_{\text{out}} = \sigma_{\text{in}}\sqrt{1+\frac{4}{\mu^2\sigma_{\text{in}}^4}}$. Here, φ_0' and α are the coefficients of the constant and second-order terms of the phase, respectively, $\varphi_0' = \varphi_0 + \omega_0\tau_0 - \frac{\pi}{4}$, $\alpha = \frac{1}{\sigma_{\text{in}}\sigma_{\text{out}}}$. According to Figure 1(b), the carrier frequency sweep rate can be denoted by the following[44]:

$$\mu = -\frac{\omega_0^3 d^2}{4\pi^2 cL}\left(1-\left(\frac{2\pi c}{\omega_0 d}-\sin\gamma\right)^2\right)^{\frac{3}{2}}, \tag{4}$$

where d is the number of grating lines. After this, the stretched laser is split into two identical beams in the BS, and these two beams with the same linear chirp will experience a time delay of τ through the delay line. When they are recombined in the BC, the two laser beams will differ by a constant frequency f_{beat}, resulting in optical heterodyning. This process generates an envelope structure as illustrated in Figure 1(b) and the beating frequency f_{beat} can be written as follows:

$$f_{\text{beat}} = \frac{\tau}{\pi\sigma_{\text{in}}\sigma_{\text{out}}} \cong \frac{\mu\tau}{2\pi}. \tag{5}$$

According to Equation (5), f_{beat} is directly proportional to the time delay τ and the linear chirp rate μ. This implies that the beating frequency can be modified by adjusting the chirp and the time delay of the two laser pulses. To simplify the analysis, we focus mainly on changing f_{beat} by adjusting τ. The envelope of Laser 2, as depicted in Figure 1(b), exhibits a periodic peak–valley structure with the beating frequency f_{beat}.

2.2. XFC amplification in the EEHG-FEL

The chirped frequency-beating laser makes it possible for us to obtain a pulse train sequence. In order to illustrate the basic process of generating an XFC using this laser, we will focus on the pulse train generation in the EEHG scheme. Following the notation of Stupakov[31], Xiang and Stupakov[32] and Kim *et al.*[45], for the hth harmonic (relative to the first seed laser), the bunching factor can be generally expressed as follows:

$$b_h = e^{im\phi}e^{-\frac{(hB_2-B_1)^2}{2}} \times J_m(-hA_2B_2)J_{-1}(-A_1(-B_1+hB_2)). \tag{6}$$

Here, ϕ is the phase difference between the two seed lasers, J_m is the mth-order Bessel function, A_1 and A_2 are the modulation intensities of the two modulation segments,

https://doi.org/10.1017/hpl.2024.37 Published online by Cambridge University Press

respectively, B_1 and B_2 are the normalized dispersion intensities of the dispersion segments, $h = m\kappa - 1$ and $\kappa = \lambda_1/\lambda_2$ is the ratio of the two seed laser wavelengths. When the second seed laser exhibits a chirp, a slight variation occurs in κ along the longitudinal direction of the laser. Consequently, h changes synchronously with κ, implying that the radiation wavelength also undergoes a slight variation. However, the impact of this small variable κ on the bunching factor b_h is negligible.

We can find the heightened sensitivity of EEHG to energy modulation from Equation (6) easily. When using a chirped frequency-beating laser as the second seed laser in the EEHG, the value of b_h is largely dependent on the modulation amplitude A_2. Hence, we can map the shape of the frequency-beating laser envelope onto the bunching distribution of the electron beam. Afterwards, the electron beam goes through the radiator to generate a pulse train sequence with a repetition frequency of f_{beat}.

However, relying solely on the frequency-beating laser to generate a pulse train sequence is insufficient to produce an XFC. Unlike the pulse train sequence generated by traditional mode-locked lasers, which maintains a consistent center frequency (wavelength), the laser pulse train sequence obtained through the aforementioned method exhibits a variable center frequency due to the introduced linear chirp during parallel gratings. According to the theory of seeded FELs, $f_{\text{fel}} = hf_{\text{seed}}$, where f_{fel} and f_{seed} represent the frequency of the FEL and the seed laser, respectively, and h represents the number of harmonic transitions. For the EEHG scheme, they share the following relationship:

$$f_{\text{fel}} = \left(m\frac{\lambda_1}{\lambda_2} - 1\right) f_{\text{seed1}} = \left(m - 1 - \frac{\lambda_2 - \lambda_1}{\lambda_1}\right) f_{\text{seed2}} \approx (m-1) f_{\text{seed2}}. \tag{7}$$

This condition holds when $m - 1 \gg \frac{\lambda_2 - \lambda_1}{\lambda_1}$, meaning that the chirp of the second seed laser is small and its central wavelength is equal to that of the first seed laser. This is consistent with the conditions of our analysis of b_h above. Consequently, the FEL also has a chirp of h times that of the second seed laser, resulting in the inability to produce a significant XFC. To overcome this problem, we have devised a method as depicted in Figure 2. By adjusting the chirp and time delay of the two laser pulses, each pulse will contain same frequency components after Fourier transformation, despite them having different center frequencies, as illustrated in Figure 3. This adjustment enables us to achieve an effect equivalent to traditional mode-locked lasers.

As illustrated in Figure 2, the basic idea of the method is to adjust the difference in frequency(Δf) between the center of neighboring pulses (e.g., f_2 and f_3) to be equal to N times the beating frequency f_{beat}, where N principally can be chosen as integers 1, 2, 3, etc. Specifically, this can be expressed by the following:

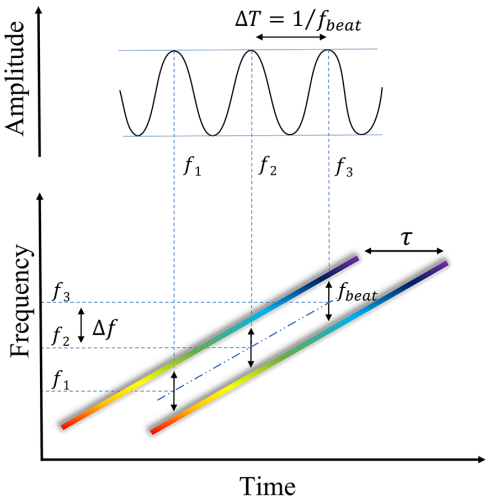

Figure 2. Schematic diagram of the chirped frequency-beating laser.

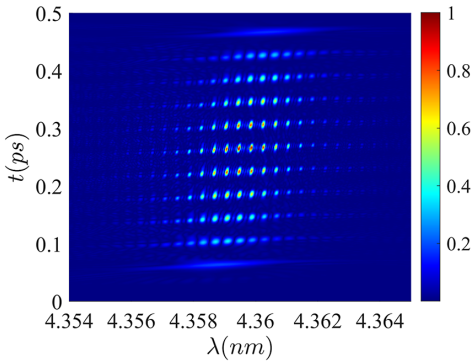

Figure 3. Wigner distribution of an XFC.

$$\Delta f = N f_{\text{beat}}. \tag{8}$$

If the carrier sweep frequency of the FEL is denoted as μ', then the frequency difference between neighboring pulses resulting from the time domain chirp of the seed laser can be expressed as follows:

$$\Delta f = \mu' \Delta t = \frac{h\mu}{2\pi} \times \frac{1}{f_{\text{beat}}}. \tag{9}$$

Bringing Equations (5) and (9) into Equation (8), the critical requirements for generating XFCs can be written as follows:

$$\tau = \sqrt{\frac{2\pi h}{\mu N}}. \tag{10}$$

When N is a positive integer, the repetition frequency of the XFC (f_{rep}) is corresponding to the beating frequency as follows: $f_{\text{rep}} = f_{\text{beat}} = \sqrt{\frac{h\mu}{2\pi N}}$. Based on this equation, achieving a lower f_{rep} for an XFC requires a reduction in the repetition frequency of the micro-pulse. Consequently, this

https://doi.org/10.1017/hpl.2024.37 Published online by Cambridge University Press

reduction leads to larger pulse widths of individual micro-pulses and a narrower bandwidth of the XFC.

To achieve an XFC with a great number of comb teeth, it is crucial to reduce the spacing between the comb teeth while broadening the spectral width. One approach is to increase the beating frequency of the seed laser to generate shorter individual micro-pulses of light. We then employ a concept akin to 'frame insertion' in image processing techniques. By systematically adjusting the central wavelength of a pulsed laser sequence, the central frequencies of some micro-pulses, upon Fourier transformation, become evenly distributed as comb teeth with intervals equal to the pulse repetition frequency (i.e., f_{beat}) in the spectra. We tentatively term this concept 'tooth insertion'. Unlike conventional mode-locked lasers, which convert only the pulse repetition frequency in the time domain into the repetition frequency of the OFC in the frequency domain, this approach allows for achieving an XFC with a P-fold increase in its repetition frequency compared to the pulse repetition frequency in the time domain. To implement 'tooth insertion', we need to modify the range of N in Equation (10). In principle, N can be any natural number (N') plus any positive fraction (P) not exceeding 1/2. Consequently, the repetition frequency of the XFC can be expressed as follows:

$$f_{\text{rep}} = Pf_{\text{beat}} = \sqrt{\frac{h\mu P^2}{2\pi N}}. \tag{11}$$

Given the limited number of pulses and the finite bandwidth of each comb in the frequency domain, N typically takes on values such as 0, 1, 2 and combinations of fractions such as 1/2, 1/3 and 1/4. The relationship among the repetition frequency f_{ref}, N and the linear chirp rate μ is illustrated in Figure 4. We can see from the figure that when μ is fixed, N can be any positive integer or its corresponding reciprocal, both corresponding to the same repetition frequency. Notably, when N is taken as 1, it corresponds to the largest repetition frequency. Moreover, if we wish to generate an XFC with a specific repetition frequency, we can choose suitable combinations of μ and N to attain the desired spectral width and tooth spacing effects for the XFC.

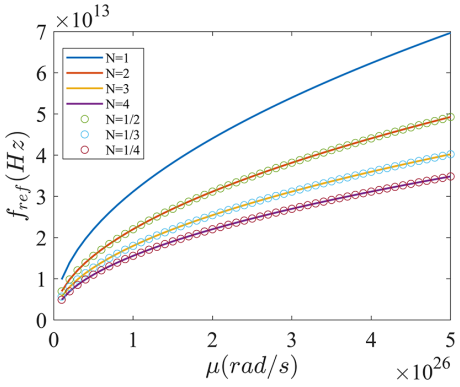

Figure 4. Repetition frequency f_{ref} with respect to N and the linear chirp rate μ.

Table 1. The parameters of the laser system.

Parameter	Value	Unit
Laser wavelength	266	nm
Laser pulse width	100	fs
Grating line	2500	mm^{-1}
Incident angle	37	°
Diffraction efficiency of a single grating	80	%
Grating pair distance	300	mm

3. Results

To demonstrate the performance of our proposed method, we have performed three-dimensional simulations with the realistic parameters of the SXFEL[41]. The FEL simulation is carried out by GENESIS1.3[46]. To achieve a relatively uniform energy modulation along the electron bunch, we employ a 3 ps laser as the first seed laser. The second seed laser is the chirped frequency-beating laser generated from the optical system depicted in Figure 1(b). The initial laser with a pulse duration of 100 fs (full width at half maximum (FWHM); the parameter will become the default in simulations and all pulse widths will be described by FWHM, unless stated otherwise for the rest of this paper) and a center wavelength of 266 nm exhibits a wavelength difference ($\Delta\lambda$) of approximately 4 nm[47]. By utilizing two parallel gratings with dispersion, the laser is stretched to 6.96 ps while simultaneously introducing a linear chirp of $\mu = 1.601 \times 10^{25}$ rad/s (the parameter will become the default in simulations unless stated otherwise). This spatiotemporally coupled laser enables the generation of a frequency-beating laser by adjusting the τ between the two lasers after the optical BS. For simulation simplicity, τ is temporarily set to 4.91 ps, corresponding to $N = 1$ in Equation (10), while the beating frequency of the laser is 12.4 THz. The simulation parameters for the laser system are outlined in Table 1, while the Wigner distribution and envelope of the chirped frequency-beating laser are illustrated in Figure 5.

The energy modulation amplitudes for EEHG are selected as $A_1 = 3$, $A_2 = 4$, corresponding to laser powers of 25.7 and 45.6 MW, respectively. For the 61st harmonic, which is corresponding to the carbon K edge (~284 eV), the optimized normalized dispersion values are estimated to be $B_1 = 16.84$, $B_2 = 0.267$. Detailed simulation parameters are presented in Table 2. Under these given parameters, the phase space of the electron beam as it traverses the modulators and chicanes is as depicted in Figure 6. Wherein, Figures 6(c) and 6(d) illustrate the phase space diagram of the electron beam modulated by the valley and peak of the laser envelope, respectively.

As depicted in Figure 7, the optimized electron beam exhibits an initial bunching of 8.5% at the 61st harmonic.

https://doi.org/10.1017/hpl.2024.37 Published online by Cambridge University Press

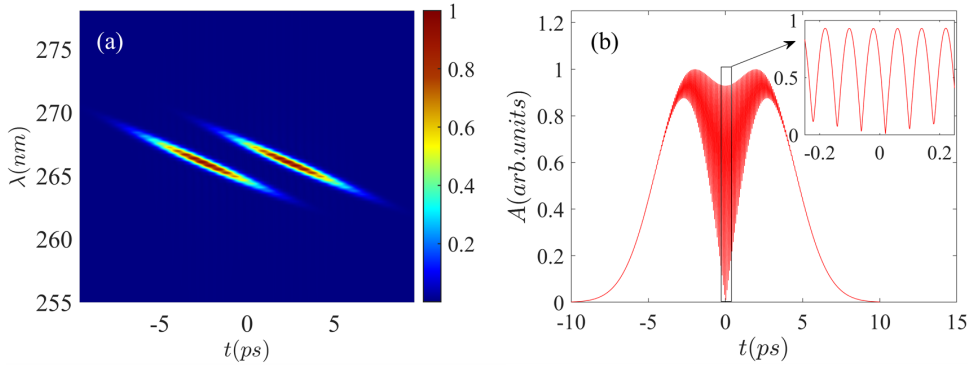

Figure 5. Schematic diagram of the Wigner distribution (a) and envelope (b) of the frequency-beating laser.

Table 2. The parameters used in the simulation.

Parameter	Value	Unit
Electron beam energy	1.5	GeV
Energy spread (rms)	60	keV
Peak current	1000	A
Bunch length	150	μm
Normalized emittance	1	mm·mrad
Wavelength of Laser 1	266	nm
Peak power of Laser 1	25.7	MW
Center wavelength of Laser 2	266	nm
Peak power of Laser 2	45.6	MW
Modulator period in M1 and M2	8	cm
Modulator period number in M1/M2	16	/
Radiator period	3	cm
Radiator period number	400	/

The electron beam then passes through the radiator, consisting of undulators with a period of 3 cm and the dimensionless undulator parameter of 1.226. In this simulation, saturation is observed at approximately 13.5 m, with a saturation power of about 600 MW. To achieve higher energy, linear asymptotic taper undulators are implemented[48,49]. As depicted in Figure 8(b), starting from a distance of 5 m from the undulator, when the taper value of the undulator is set to 0.01, the peak power of the FEL reaches approximately 1.5 GW at the same distance of 13.5 m. This represents an approximately 2.5-fold increase compared to the absence of taper undulators. Figure 8(a) illustrates that the frequency spacing between adjacent teeth of the XFC is around 12.4 THz. Furthermore, it can be observed that the spectra of the FELs are minimally affected by the taper undulator, indicating that this approach is an effective method for generating high-intensity XFCs.

We want to emphasize that the optimization condition in Equation (10) is critical in the generation of ideal XFCs. We conduct another simulation with the same parameters above except that the time delay τ is 5.50 ps rather than the optimized value of 4.91 ps, and the results are shown in Figure 9. We can see that the radiation spectrum exhibits numerous spurious peaks and lacks the characteristic evenly spaced frequency teeth in XFCs.

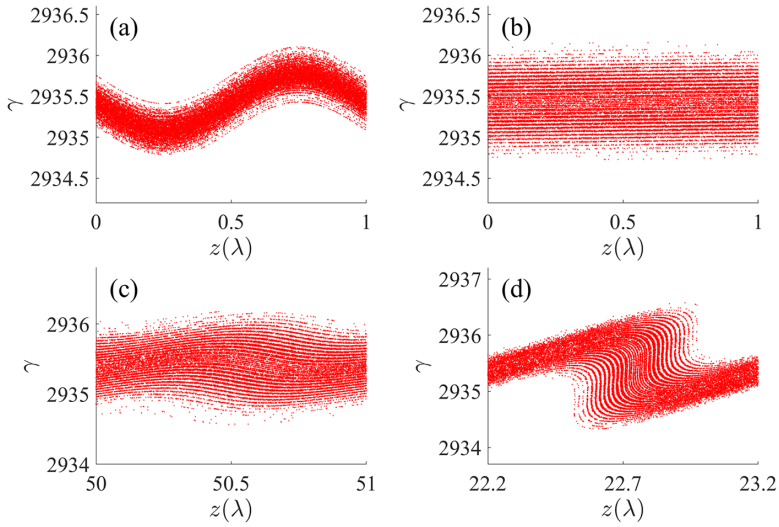

Figure 6. Longitudinal phase space evolution. Schematic of the phase space of electron beams in the scheme: after Modulator 1 (a), after Chicane 1 (b) and after Chicane 2 (c), (d).

https://doi.org/10.1017/hpl.2024.37 Published online by Cambridge University Press

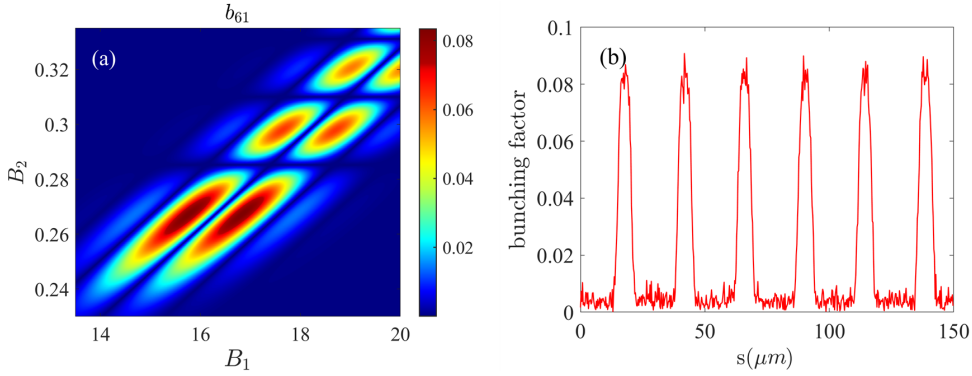

Figure 7. Bunching optimization of EEHG for $A_1 = 3$ and $A_2 = 4$ (a) and the initial bunching factor distribution of the electron beam (b).

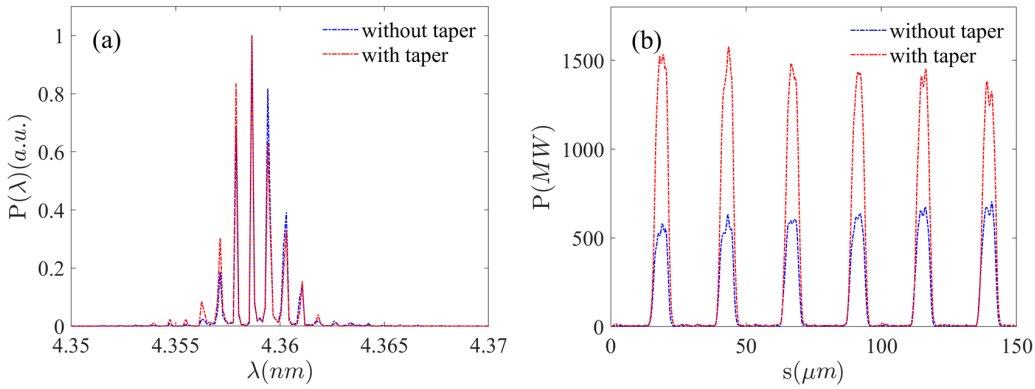

Figure 8. Radiation performance of the proposed method. Spectra (a) and saturation power distributions (b) of the XFC.

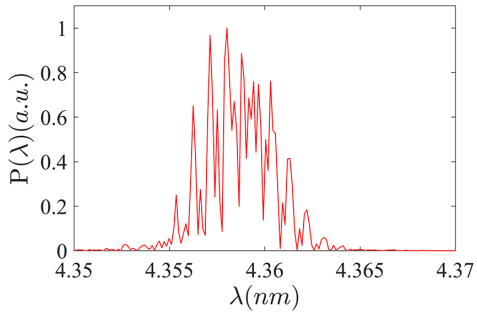

Figure 9. Radiation spectrum when the time delay τ is 5.50 ps rather than the optimized value of 4.91 ps.

To validate the accuracy and efficacy of our proposed method, we also conducted simulations with $N = 2$, according to Equation (10). In this case, the corresponding time delay τ is 3.47 ps, with the corresponding repetition frequency being 8.79 THz. The results are presented in Figures 10(a) and 10(c). From Figure 10(c), it is evident that it achieves efficient mode-locked amplification and generates an XFC with varying integer values of N. This observation serves as robust confirmation for our previously derived Equations (10) and (11). However, the XFC in Figure 10(c) consists of only a few comb teeth. The limitation arises primarily due to the continuous envelope of the frequency-beating laser, which restricts the ability to adjust the ratio of individual pulse duration to neighboring pulse duration. Consequently, the spectral width of the XFC and the number of comb teeth are both limited. For instance, when $N = 2$, corresponding to $f_{\text{rep}} = 8.79$ THz, despite the insensitivity of the scheme to the slippage effect of the FEL, the FWHM length of a single micro-pulse still extends to 23.3 fs, resulting in a significantly narrower spectral width after Fourier transform. Improvements can be made by increasing the number of micro-pulses appropriately based on the chirp characteristics of the seed laser. In addition, modifications to the ratio of A_1 to A_2 can also be considered, considering the sensitivity of the EEHG to energy modulation. However, it is crucial to recognize that these adjustments have limitations.

To demonstrate the possibility of Equation (11), we also simulated the case when $N = 1/2$, also corresponding to the repetition frequency of 8.79 THz. The simulation results are depicted in Figures 10(b) and 10(d). Comparing the spectra of $N = 2$ with those of $N = 1/2$, the simulation results reveal that the 'tooth insertion' method expands the bandwidth of the XFC while maintaining the repetition frequency. The reason is that, as f_{beat} increases, the pulse width of a single micro-pulse decreases, as shown in Figures 10(a) and 10(c). However, there are limitations to this method. Firstly, it may result in blurred boundaries of the comb teeth, particularly at the end of the XFC. This issue can be effectively mitigated by increasing the number of micro-pulses. Secondly, the choice of a smaller fraction P, which corresponds to a larger repetition frequency, is fundamentally limited by the mini-

https://doi.org/10.1017/hpl.2024.37 Published online by Cambridge University Press

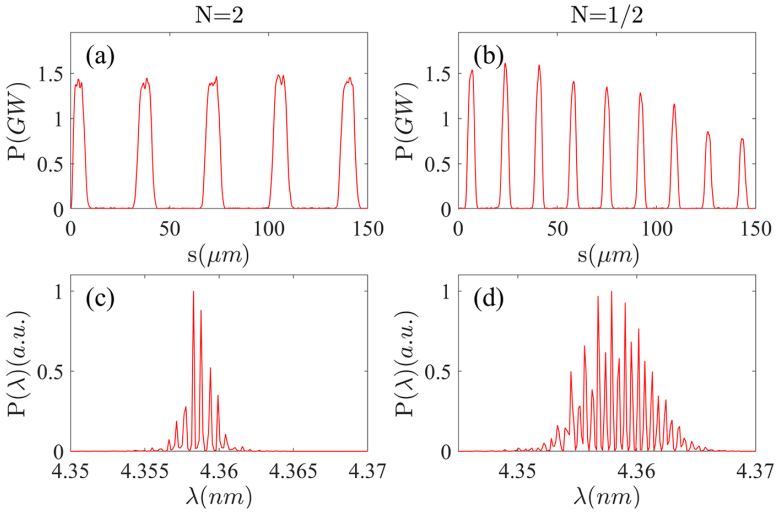

Figure 10. Power and spectrum distributions of the XFCs when $N = 2$ and $N = 1/2$.

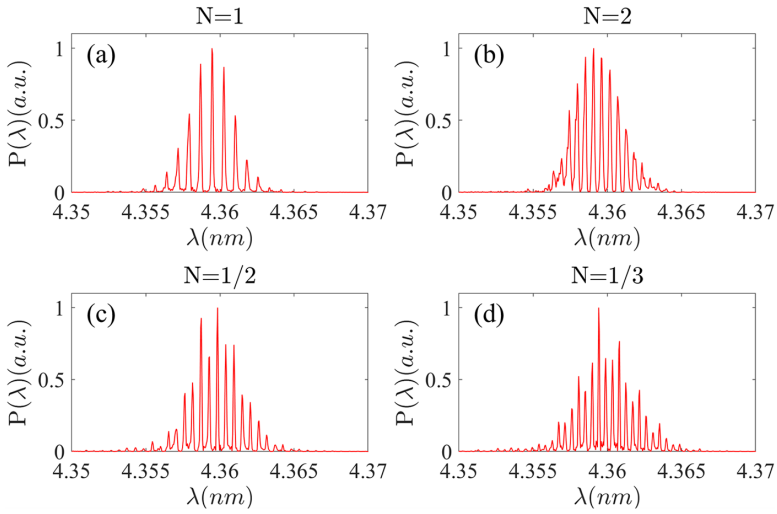

Figure 11. Spectra of the XFCs when an initial 30 fs laser is used.

mum bandwidth of the initial ultrafast laser. The wavelength difference contained in this initial ultrafast laser affects the maximum chirp and the maximum pulse width of the laser after passing through the dispersive medium. Therefore, the narrower the initial laser pulse width, the larger the tunable range of the XFC.

To validate our assertion, an ultrafast laser with a duration of 30 fs is also used in the simulation and the result is shown in Figure 11. As observed from the figure, the spectral structure is greatly improved by using a shorter initial laser.

Since the critical optimization conditions for generating the XFCs are necessary in the proposed method, we simulated the scenario when the relative time delay deviates ± 100 fs from the optimized value of 4.91 ps for $N = 1$ to evaluate the impact. The results indicate that under these circumstances, an X-ray spectral comb can still be maintained, as shown in Figure 12. This proves the proposed scheme is quite robust, as normally the time drift in this seed laser system should be only a few femtoseconds.

4. Discussion and conclusions

This study presents a feasible method for achieving continuous tunable XFCs using the chirped frequency-beating laser technique in a seeded FEL. By manipulating the Wigner distribution and beating frequency of the seed laser, a suitable seed signal for generating the XFC can be generated. This seed signal is effectively preserved and amplified in the EEHG-FEL process, resulting in high-power XFC output. With this method, it becomes feasible to generate a tunable repetition frequency XFC with a peak power of 1.5 GW, using a 100 fs initial conventional laser. We want to mention that the repetition frequency of the XFCs in our method

https://doi.org/10.1017/hpl.2024.37 Published online by Cambridge University Press

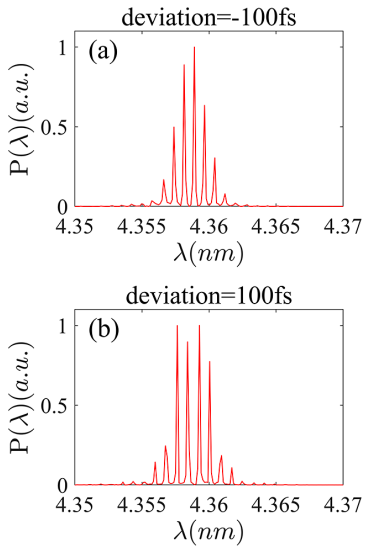

Figure 12. XFC radiation spectra with the relative time delay deviating ±100 fs from the optimized value of 4.91 ps for $N = 1$.

can be tuned easily by manipulating the linear chirp μ and the relative time delay τ in the frequency-beating seed laser system. By appropriately setting these parameters, the XFC spectra can be broadened and the number of comb teeth can be increased to dozens. In addition, by employing an initial laser with a shorter pulse duration, the bandwidth and the number of comb teeth can be further augmented. Furthermore, we are planning to validate this method experimentally in the SXFEL. Although the experiment faces challenges, such as the limitation of the maximum modulation intensity that can be provided by a chirped frequency-beating laser, preparations for the experimental conditions are currently underway, particularly for the chirped frequency-beating seed laser system. We anticipate that implementing this approach will significantly enhance the capabilities of seeded FELs for conducting spectroscopic experiments.

Acknowledgements

The authors thank Yiwen Liu, Yin Kang, Weijie Fan and Hao Sun for helpful discussions and useful comments. This work was supported by the National Natural Science Foundation of China (No. 12122514), Zhangjiang Laboratory, Project for Young Scientists in Basic Research of the Chinese Academy of Sciences (No. YSBR-091) and the Strategy Priority Research Program of the Chinese Academy of Sciences (No. XDB0530300).

References

1. T. Udem, R. Holzwarth, and T. W. Hänsch, Nature **416**, 233 (2002).
2. S. A. Diddams, T. Udem, J. C. Bergquist, E. A. Curtis, R. Drullinger, L. Hollberg, W. M. Itano, W. D. Lee, C. W. Oates, K. R. Vogel, and D. J. Wineland, Science **293**, 825 (2001).
3. S. M. Cavaletto, Z. Harman, C. Ott, C. Buth, T. Pfeifer, and C. H. Keitel, Nat. Photonics **8**, 520 (2014).
4. I. Coddington, N. Newbury, and W. Swann, Optica **3**, 414 (2016).
5. T. Wilken, G. L. Curto, R. A. Probst, T. Steinmetz, A. Manescau, L. Pasquini, J. I. G. Hernández, R. Rebolo, T. W. Hänsch, T. Udem, and R. Holzwarth, Nature **485**, 611 (2012).
6. M. T. Murphy, T. Udem, R. Holzwarth, A. Sizmann, L. Pasquini, C. Araujo-Hauck, H. Dekker, S. D'Odorico, M. Fischer, T. W. Hänsch, and A. Manescau, Mon. Not. R Astron. Soc. **380**, 839 (2007).
7. M. Tan, X. Xu, A. Boes, B. Corcoran, J. Wu, T. G. Nguyen, S. T. Chu, B. E. Little, R. Morandotti, A. Mitchell, and D. J. Moss, J. Lightwave Technol. **38**, 6221 (2020).
8. D. A. Braje, M. S. Kirchner, S. Osterman, T. Fortier, and S. A. Diddams, Eur. Phys. J. D **48**, 57 (2008).
9. Y. Geng, X. Huang, W. Cui, Y. Ling, B. Xu, J. Zhang, X. Yi, B. Wu, S.-W. Huang, K. Qiu, C. W. Wong, and H. Zhou, Opt. Lett. **43**, 2406 (2018).
10. R. Zhou, S. Latkowski, J. O'Carroll, R. Phelan, L. P. Barry, and P. Anandarajah, Opt. Express **19**, B415 (2011).
11. L. J. P. Ament, M. van Veenendaal, T. P. Devereaux, J. P. Hill, and J. van den Brink, Rev. Mod. Phys. **83**, 705 (2011).
12. J. Pfeifle, V. Brasch, M. Lauermann, Y. Yu, D. Wegner, T. Herr, K. Hartinger, P. Schindler, J. Li, D. Hillerkuss, R. Schmogrow, C. Weimann, R. Holzwarth, W. Freude, J. Leuthold, T. J. Kippenberg, and C. Koos, Nat. Photonics **8**, 375 (2014).
13. F. Quinlan, S. Ozharar, S. Gee, and P. J. Delfyett, J. Opt. A: Pure Appl. Opt. **11**, 103001 (2009).
14. T. Jung, J.-L. Shen, D. T. K. Tong, S. Murthy, M. C. Wu, T. Tanbun-Ek, W. Wang, R. Lodenkamper, R. Davis, L. J. Lembo, and J. C. Brock, IEEE Trans. Microw. Theory Tech. **47**, 1225 (1999).
15. X. F. Li, A. l'Huillier, M. Ferray, L. A. Lompré, and G. Mainfray, Phys. Rev. A **39**, 5751 (1989).
16. D. C. Yost, T. R. Schibli, J. Ye, J. L. Tate, J. Hostetter, M. B. Gaarde, and K. J. Schafer, Nat. Phys. **5**, 815 (2009).
17. D. C. Yost, A. Cingöz, T. K. Allison, A. Ruehl, M. E. Fermann, I. Hartl, and J. Ye, Opt. Express **19**, 23483 (2011).
18. H. S. Kang, J. Korean Phys. Soc. **80**, 684 (2022).
19. P. Emma, R. Akre, J. Arthur, R. Bionta, C. Bostedt, J. Bozek, A. Brachmann, P. Bucksbaum, R. Coffee, F.-J. Decker, Y. Ding, D. Dowell, S. Edstrom, A. Fisher, J. Frisch, S. Gilevich, J. Hastings, G. Hays, P. Hering, Z. Huang, R. Iverson, H. Loos, M. Messerschmidt, A. Miahnahri, S. Moeller, H.-D. Nuhn, G. Pile, D. Ratner, J. Rzepiela, D. Schultz, T. Smith, P. Stefan, H. Tompkins, J. Turner, J. Welch, W. White, J. Wu, G. Yocky, and J. Galayda, Nat. Photonics **4**, 641 (2010).
20. S. Gerber, H. Jang, H. Nojiri, S. Matsuzawa, H. Yasumura, D. A. Bonn, R. Liang, W. N. Hardy, Z. Islam, A. Mehta, S. Song, M. Sikorski, D. Stefanescu, Y. Feng, S. A. Kivelson, T. P. Devereaux, Z.-X. Shen, C.-C. Kao, W.-S. Lee, D. Zhu, and J.-S. Lee, Science **350**, 949 (2015).
21. Y. Kang, X. E. Zhou, X. Gao, Y. He, W. Liu, A. Ishchenko, A. Barty, T. A. White, O. Yefanov, G. W. Han, Q. Xu, P. W. de Waal, J. Ke, M. H. E. Tan, C. Zhang, A. Moeller, G. M. West, B. D. Pascal, N. Van Eps, L. N. Caro, S. A. Vishnivetskiy, R. J. Lee, K. M. Suino-Powell, X. Gu, K. Pal, J. Ma, X. Zhi, S. Boutet, G. J. Williams, M. Messerschmidt, C. Gati, N. A. Zatsepin, D. Wang, D. James, S. Basu, S. Roy-Chowdhury, C. E. Conrad, J. Coe, H. Liu, S. Lisova, C. Kupitz, I. Grotjohann, R. Fromme, Y. Jiang, M. Tan, H. Yang, J. Li, M. Wang, Z. Zheng, D. Li, N. Howe, Y. Zhao, J. Standfuss, K. Diederichs, Y. Dong, C. S. Potter, B. Carragher, M. Caffrey, H. Jiang, H. N. Chapman, J. C. H. Spence, P. Fromme, U. Weierstall, O. P.

https://doi.org/10.1017/hpl.2024.37 Published online by Cambridge University Press

Ernst, V. Katritch, V. V. Gurevich, P. R. Griffin, W. L. Hubbell, R. C. Stevens, V. Cherezov, K. Melcher, and H. E. Xu, Nature **523**, 561 (2015).
22. H. Öström, H. Öberg, H. Xin, J. LaRue, M. Beye, M. Dell'Angela, J. Gladh, M. L. Ng, J. A. Sellberg, S. Kaya, G. Mercurio, D. Nordlund, M. Hantschmann, F. Hieke, D. Kühn, W. F. Schlotter, G. L. Dakovski, J. J. Turner, M. P. Minitti, A. Mitra, S. P. Moeller, A. Föhlisch, M. Wolf, W. Wurth, M. Persson, J. K. Nørskov, F. Abild-pedersen, H. Ogasawara, L. G. M. Pettersson, and A. Nilsson, Science **347**, 978 (2015).
23. J. M. J. Madey, J. Appl. Phys. **42**, 1906 (1971).
24. A. M. Kondratenko and E. L. Saldin, Part. Accel. **10**, 207 (1980).
25. R. Bonifacio, C. Pellegrini, and L. M. Narducci, Opt. Commun. **50**, 373 (1984).
26. J. Feldhaus, E. L. Saldin, J. R. Schneider, E. A. Schneidmiller, and M. V. Yurkov, Opt. Commun. **140**, 341 (1997).
27. G. Geloni, V. Kocharyan, and E. Saldin, J. Mod. Opt. **58**, 1391 (2011).
28. C. Feng and H. X. Deng, Nucl. Sci. Techn. **29**, 214 (2018).
29. L. H. Yu, Phys. Rev. A **44**, 5178 (1991).
30. L. H. Yu and J. Wu, Nucl. Instrum. Methods Phys. Res. A **483**, 493 (2002).
31. G. Stupakov, Phys. Rev. Lett. **102**, 074801 (2009).
32. D. Xiang and G. Stupakov, Phys. Rev. Spec. Top. Accel. Beams **12**, 030702 (2009).
33. Z. T. Zhao, D. Wang, J. H. Chen, Z. H. Chen, H. X. Deng, J. G. Ding, C. Feng, Q. Gu, M. M. Huang, T. H. Lan, Y. B. Leng, D. G. Li, G. Q. Lin, B. Liu, E. Prat, X. T. Wang, Z. S. Wang, K. R. Ye, L. Y. Yu, H. O. Zhang, J. Q. Zhang, M. Zhang, M. Zhang, T. Zhang, S. P. Zhong, and Q. G. Zhou, Nat. Photonics **6**, 360 (2012).
34. P. R. Ribič, A. Abrami, L. Badano, M. Bossi, H.-H. Braun, N. Bruchon, F. Capotondi, D. Castronovo, M. Cautero, P. Cinquegrana, M. Coreno, M. E. Couprie, I. Cudin, M. B. Danailov, G. De Ninno, A. Demidovich, S. Di Mitri, B. Diviacco, W. M. Fawley, C. Feng, M. Ferianis, E. Ferrari, L. Foglia, F. Frassetto, G. Gaio, D. Garzella, A. Ghaith, F. Giacuzzo, L. Giannessi, V. Grattoni, S. Grulja, E. Hemsing, F. Iazzourene, G. Kurdi, M. Lonza, N. Mahne, M. Malvestuto, M. Manfredda, C. Masciovecchio, P. Miotti, N. S. Mirian, I. P. Nikolov, G. M. Penco, G. Penn, L. Poletto, M. Pop, E. Prat, E. Principi, L. Raimondi, S. Reiche, E. Roussel, R. Sauro, C. Scafuri, P. Sigalotti, S. Spampinati, C. Spezzani, L. Sturari, M. Svandrlik, T. Tanikawa, M. Trovó, M. Veronese, D. Vivoda, D. Xiang, M. Zaccaria, D. Zangrando, M. Zangrando, and E. M. Allaria, Nat. Photonics **13**, 555 (2019).
35. C. Feng, H. Deng, M. Zhang, X. Wang, S. Chen, T. Liu, K. Zhou, D. Gu, Z. Wang, Z. Jiang, X. Li, B. Wang, W. Zhang, T. Lan, L. Feng, B. Liu, Q. Gu, Y. Leng, L. Yin, D. Wang, Z. Zhao, G. Wang, and D. Xiang, Phys. Rev. Accel. Beams **22**, 050703 (2019).
36. C. Feng, T. Liu, S. Chen, K. Zhou, K. Zhang, Z. Qi, D. Gu, Z. Wang, Z. Jiang, X. Li, B. Wang, X. Wang, W. Zhang, L. Feng, C. Li, T. Lan, B. Li, M. Zhang, H. Deng, D. Xiang, B. Liu, and Z. Zhao, Optica **9**, 785 (2022).
37. D. Xiang, Y. Ding, T. Raubenheimer, and J. Wu, Phys. Rev. Spec. Top. Accel. Beams **15**, 050707 (2012).
38. C. Feng, J. Chen, and Z. Zhao, Phys. Rev. Spec. Top. Accel. Beams **15**, 080703 (2012).
39. P. K. Maroju, C. Grazioli, M. Di Fraia, M. Moioli, D. Ertel, H. Ahmadi, O. Plekan, P. Finetti, E. Allaria, L. Giannessi, G. De Ninno, C. Spezzani, G. Penco, S. Spampinati, A. Demidovich, M. B. Danailov, R. Borghes, G. Kourousias, C. E. Sanches Dos Reis, F. Billé, A. A. Lutman, R. J. Squibb, R. Feifel, P. Carpeggiani, M. Reduzzi, T. Mazza, M. Meyer, S. Bengtsson, N. Ibrakovic, E. R. Simpson, J. Mauritsson, T. Csizmadia, M. Dumergue, S. Kühn, H. N. Gopalakrishna, D. You, K. Ueda, M. Labeye, J. E. Bækhøj, K. J. Schafer, E. V. Gryzlova, A. N. Grum-Grzhimailo, K. C. Prince, C. Callegari, and G. Sansone, Nature **578**, 386 (2020).
40. X. Xu, H. Zhang, B. Li, C. Li, Z. Guo, J. Li, and Z. He, Nucl. Instrum. Methods Phys. Res. A **1055**, 168530 (2023).
41. B. Liu, C. Feng, D. Gu, F. Gao, H. Deng, M. Zhang, S. Sun, S. Chen, W. Zhang, W. Fang, Z. Wang, Q. Zhou, Y. Leng, M. Gu, L. Yin, Q. Gu, G. Fang, D. Wang, and Z. Zhao, Appl. Sci. **12**, 176 (2021).
42. Y. Kang, Z. Wang, K. Zhang, and C. Feng, Photonics **10**, 133 (2023).
43. K. Zhang, Y. Kang, T. Liu, Z. Wang, C. Feng, W. Fang, and Z. Zhao, Appl. Sci. **11**, 11850 (2021).
44. A. S. Weling and D. H. Auston, J. Opt. Soc. Am. B **13**, 2783 (1996).
45. K.-J. Kim, Z. Huang, and R. Lindberg, *Synchrotron Radiation and Free-Electron Lasers* (Cambridge University Press, Cambridge, 2017), p. 190.
46. S. Reiche, Nucl. Instrum. Methods Phys. Res A **429**, 243 (1999).
47. Y. Xiao, C. Feng, and B. Liu, Ultrafast Sci. **2022**, 9812478 (2022).
48. Y. Jiao, J. Wu, Y. Cai, A. W. Chao, W. M. Fawley, J. Frisch, Z. Huang, H. D. Nuhn, C. Pellegrini, and S. Reiche, Phys. Rev. Spec. Top. Accel. Beams **15**, 050704 (2012).
49. E. A. Schneidmiller, Phys. Rev. Accel. Beams **25**, 010701 (2022).

https://doi.org/10.1017/hpl.2024.37 Published online by Cambridge University Press